

# INHOMOGENEOUS STELLAR MODELS. I. MODELS WITH A CONVECTIVE CORE AND A DISCONTINUITY IN THE CHEMICAL COMPOSITION\*

J. B. OKE AND M. SCHWARZSCHILD

Princeton University Observatory

*Received April 16, 1952*

## ABSTRACT

A number of stellar models with a discontinuity in chemical composition have been computed through in detail. An arbitrary, but fixed, hydrogen-poor composition was used for the interior of all models, and a fixed hydrogen-rich composition was similarly used for all envelopes. The position in the star at which the change in chemical composition occurs was varied over a wide range. The computed models were found to cover well the observed red giants, as far as radii and luminosities are concerned. The masses of the theoretical red-giant models, however, fall systematically somewhat below the standard mass-luminosity relation—a circumstance not necessarily in discordance with observation.

## I. INTRODUCTION

Since 1938 inhomogeneous stellar models have been investigated in a number of papers.<sup>1</sup> The main conclusion appears to be that inhomogeneities in the interior chemical composition may be the main cause for the large radii of the red giants. The question, however, of exactly what types of inhomogeneities are needed to explain the observed characteristics of the red giants and how these specific inhomogeneities might arise during the evolution of a red giant still appears to need further investigation.

In a recent paper<sup>2</sup> a series of models containing a convective core and a discontinuity in the chemical composition were computed. These computations were restricted to cases with only moderate deviations from the observed mass-luminosity relation. This restriction has been criticized<sup>3</sup> on the basis of the uncertainties in the few observed masses of red giants. This criticism has since gained strength by the circumstance that the mass of Capella, formerly considered a first-class datum, has recently been shown<sup>4</sup> to be quite uncertain.

In the present paper are given two series of models with a convective core and a chemical discontinuity—without regard to deviations from the empirical mass-luminosity law. The two series differ in the assumed variation of the absorption coefficient in the deep interior. The individual models in each series differ from one another in the percentage of the total mass contained in the hydrogen-poor interior portion of the star. All models of this paper were chosen to have the same hydrogen-poor composition in the interior and the same hydrogen-rich composition in the envelope. As in several of the

\* This research was supported in part by funds of the Eugene Higgins Trust allocated to Princeton University and in part by contract with the Office of Naval Research.

<sup>1</sup> E. Öpik, *Pub. Obs. Tartu*, Vol. 30, Nos. 3 and 4, 1938; 31, No. 1, 1943; *Armagh Obs. Contr.*, No. 2, 1949; No. 3, 1951. G. Gamow, *Ap. J.*, 87, 206, 1938. C. L. Critchfield and G. Gamow, *Ap. J.*, 89, 244, 1939. S. Chandrasekhar and L. R. Henrich, *Ap. J.*, 94, 525, 1941. M. Schönberg and S. Chandrasekhar, *Ap. J.*, 96, 161, 1942. F. Hoyle and R. A. Lyttleton, *M.N.*, 102, 218, 1942; 109, 614, 1949. M. H. Harrison, *Ap. J.*, 100, 343, 1944; 103, 192, 1946; 105, 322, 1947. G. Gamow and G. Keller, *Rev. Mod. Phys.*, 17, 125, 1945. A. Reiz, *Ann. d'ap.*, 10, 301, 1947. P. Ledoux, *Ap. J.*, 105, 305, 1947; *Ann. d'ap.*, 11, 174, 1948. Li Hen and M. Schwarzschild, *M.N.*, 109, 631, 1949. C. M. Bondi, *M.N.*, 110, 275, 1950. C. M. Bondi and H. Bondi, *M.N.*, 110, 287, 1950; 111, 397, 1951. J. G. Gardiner, *M.N.*, 111, 102, 1951.

<sup>2</sup> Li Hen and M. Schwarzschild, *op. cit.*

<sup>3</sup> C. M. Bondi and H. Bondi, *M.N.*, 110, 287, 1950.

<sup>4</sup> O. Struve, *Proc. Nat. Acad. Sci.*, 37, 327, 1951.

earlier investigations, it was again arbitrarily assumed here that the composition in the deep interior, though hydrogen-poor, contained sufficient hydrogen to feed the nuclear energy sources in the core.

## II. ASSUMPTIONS AND BASIC EQUATIONS

The models here considered consist of a hydrogen-rich envelope and a hydrogen-poor interior, the latter of which is divided into a radiative intermediate zone and a convective core. To simplify the computations, it has been assumed (a) that radiation pressure and degeneracy are negligible, (b) that electron scattering can be ignored, and (c) that the entire energy generation occurs within the convective core.

The computations have been carried out with help of the following definitions and equations:

### *Subscripts:*

- e*, envelope; *i*, interior; *c*, center;  
 1, inner interface, between the convective core and the radiative intermediate zone;  
 2, outer interface, between the radiative intermediate zone and the envelope.

### *Absorption coefficient:*

$$\kappa = \frac{\kappa_0}{(t/\bar{g})} \rho T^{-3.5} \quad \text{with} \quad \kappa_0 = 4 \times 10^{25} Z (1 + X), \quad (1)$$

where the guillotine factor is given by

$$\frac{t}{\bar{g}} = \left( \frac{t}{\bar{g}} \right)_0 \left( \frac{\rho}{\rho_{2i}} \right)^\alpha, \quad (2)$$

with  $\alpha = 0$  in the envelope of both model series and in the interior of the first model series, but with  $\alpha = 0.25$  in the interior of the second model series.

### *Dimensionless variables:*

$$P = \dot{p} \frac{GM^2}{4\pi R^4}, \quad T = t \frac{\mu_e H GM}{k R}, \quad M_r = qM, \quad r = xR. \quad (3)$$

### *Composition parameters:*

$$l = \frac{\mu}{\mu_e} = \frac{2X_e + \frac{3}{4}Y_e + \frac{1}{2}Z_e}{2X + \frac{3}{4}Y + \frac{1}{2}Z}, \quad j = \frac{Z}{Z_e} \frac{1+X}{1+X_e} \frac{\mu}{\mu_e}. \quad (4)$$

Appropriate relation if  $Z = Z_e$ :  $j = l^{0.30}$ .

In envelope, by definition:  $l_e = j_e = 1$ .

In interior, by assumption:  $l_i = 2.5$ ,  $j_i = 1.316$ .

### *Basic equations for radiative parts:*

$$\frac{d\dot{p}}{dx} = -l \frac{\dot{p}q}{x^2 t}, \quad \frac{dq}{dx} = +l \frac{\dot{p}x^2}{t}, \quad (5)$$

$$\frac{dt}{dx} = -ljC \left( \frac{\dot{p}_{2i}}{t_{2i}} \right)^\alpha \frac{\dot{p}^{2-\alpha}}{x^2 t^{3.5-\alpha}}, \quad (6)$$

with

$$C = \frac{3}{4ac} \left( \frac{k}{\mu_e HG} \right)^{7.5} \left( \frac{1}{4\pi} \right)^3 \frac{\kappa_0}{(t/\bar{g})_0} \frac{LR^{0.5}}{M^{5.5}}. \quad (7)$$

*Homology invariants:*

$$U = l \frac{p x^3}{t q}, \quad V = l \frac{q}{t x}, \quad n + 1 = \frac{1}{j C} \left( \frac{t_{2i}}{p_{2i}} \right)^a \frac{q t^{8.5-a}}{p^{2-a}}. \quad (8)$$

*Emden variables for convective core:*

$$t = \theta t_c, \quad p = \theta^{n+1} p_c, \quad x = \xi \frac{x_1}{\xi_1}. \quad (9)$$

In core, by assumption:  $\gamma = \frac{5}{3}$  or  $n = 1.5$ .

*Fitting conditions at discontinuity:*

$$\frac{U_{2i}}{U_{2e}} = \frac{V_{2i}}{V_{2e}} = \frac{l_i}{l_e} = 2.5, \quad \frac{n_{2e} + 1}{n_{2i} + 1} = \frac{j_i}{j_e} = 1.316. \quad (10)$$

### III. CONSTRUCTION OF THE MODELS

The numerical solutions needed for the three parts of the model were obtained as follows.

In the envelope where Kramers' law was assumed for the absorption coefficient ( $\alpha = 0$ ), the differential equations (5) and (6), together with the usual boundary conditions ( $p = t = 0, q = 1$  for  $x = 1$ ), define a single-parameter family of solutions depending only on the value of  $C$ . Ten particular solutions of this family, covering a range in  $\log C$  from  $-1$  to  $-7$ , were obtained by numerical integrations.<sup>5</sup>

For the convective core, the one solution needed, which has no singularity at the center, is available in tabular form.<sup>6</sup>

For the intermediate zone, equations (5) and (6), together with the condition of a continuous fit at the boundary of the convective core, give a single-parameter family of solutions. Each particular solution of this family is characterized by a value of the independent Emden variable,  $\xi_1$ , which gives the point at which the convective core is terminated and the intermediate radiative zone is started. A method of obtaining starting values for these solutions by applying the appropriate fitting conditions at the surface of the convective core has been described previously.<sup>2</sup> Five particular solutions covering the necessary range in  $\xi_1$  were obtained by numerical integration<sup>5</sup> under the assumption of  $\alpha = 0$ . These solutions were used for the construction of the first series of models. For the second series, for which  $\alpha = 0.25$  was taken in the intermediate zone, a set of numerical integrations for the intermediate zone was already available.<sup>2</sup>

All the numerical solutions used are shown in Figure 1 in terms of the homology invariants  $U$  and  $V$ . The two halves of this figure correspond separately to the two series of models.

To complete the models, it remains to fit the intermediate zones to the envelopes under the conditions of equations (10). This fitting can conveniently be done with the help of the  $U$ - $V$  plane, as shown in Figure 1. If one arbitrarily selects a particular solution for the intermediate zone and if, further, one selects a particular point on this solution for the outer boundary of the intermediate zone, one can read off directly  $U_{2i}$  and  $V_{2i}$ . The starting point for the corresponding envelope solution in the  $U$ - $V$  plane ( $U_{2e}, V_{2e}$ ) can then be obtained from the first of equations (10). The jump from the point ( $U_{2i}, V_{2i}$ ) to the point ( $U_{2e}, V_{2e}$ ) is represented in the  $U$ - $V$  plane by a straight line pointing to the origin. In general, however, this procedure will not permit the second equation

<sup>5</sup> To be published in a forthcoming *Princeton U. Obs. Contr.*

<sup>6</sup> *Brit. Assoc. Adv. Sci., Math. Tables*, Vol. 2, 1932.



(10) to be fulfilled; the value of  $n_{2i}$  corresponding to the point  $(U_{2i}, V_{2i})$  can be obtained from the intermediate-zone solutions (or by interpolation between them), and similarly the value of  $n_{2e}$  corresponding to the point  $(U_{2e}, V_{2e})$  can be obtained by interpolation between the envelope solutions. In general, these two values of  $n$  will not fulfil the second condition (10) but will do so only for one specific point on each intermediate-zone solution. This specific point was determined for each of the numerical solutions for the intermediate zone by graphical interpolation, together with the corresponding point on the envelope solutions. Each such pair of points is shown in Figure 1 by a straight line connecting them. Any such jump line represents one particular model and is designated by

TABLE 1  
MATHEMATICAL CHARACTERISTICS OF FIRST-MODEL SERIES

	I	II	III	IV	V	VI	VII
$\xi_1$ .....	+1.21	+1.194	+1.193	+1.1925	+1.19232	+1.192315	+1.192309
$U_1$ .....	+2.57	+2.582	+2.583	+2.583	+2.583	+2.583	+2.583
$V_1$ .....	+1.26	+1.224	+1.222	+1.220	+1.220	+1.220	+1.220
$U_{2e}$ .....	+0.720	+0.507	+0.435	+0.343	+0.218	+0.181	+0.141
$V_{2e}$ .....	+1.428	+2.070	+2.306	+2.652	+3.267	+3.501	+3.844
$(n+1)_{2e}$ .....	+3.290	+3.727	+3.839	+3.965	+4.107	+4.141	+4.174
$\log C$ .....	-5.37	-4.89	-4.67	-4.32	-3.44	-3.00	-2.50
$\log t_2$ .....	+0.150	+0.331	+0.420	+0.583	+0.995	+1.128	+0.985
$\log p_2$ .....	+2.635	+3.249	+3.543	+4.098	+5.487	+5.868	+5.070
$\log q_2$ .....	-0.857	-0.636	-0.568	-0.480	-0.313	-0.233	-0.113
$\log x_2$ .....	-1.162	-1.283	-1.351	-1.487	-1.822	-1.905	-1.683
$\log t_2/t_1$ .....	-0.17	-0.289	-0.332	-0.394	-0.505	-0.547	-0.604
$\log t_1$ .....	+0.32	+0.620	+0.752	+0.977	+1.500	+1.675	+1.589
$\log p_1$ .....	+3.10	+4.170	+4.635	+5.441	+7.284	+7.842	+7.282
$\log q_1$ .....	-1.35	-1.303	-1.273	-1.227	-1.103	-1.032	-0.924
$\log x_1$ .....	-1.37	-1.613	-1.714	-1.892	-2.291	-2.395	-2.201
$\log t_c$ .....	+0.43	+0.725	+0.857	+1.082	+1.605	+1.780	+1.694
$\log p_c$ .....	+3.37	+4.432	+4.896	+5.702	+7.545	+8.103	+7.543
$q_1 = M_1/M$ .....	+0.044	+0.050	+0.053	+0.059	+0.079	+0.093	+0.119
$q_2 = M_2/M$ .....	+0.139	+0.231	+0.270	+0.331	+0.486	+0.585	+0.771
$x_1 = r_1/R$ .....	+0.043	+0.024	+0.019	+0.013	+0.005	+0.004	+0.006
$x_2 = r_2/R$ .....	+0.069	+0.052	+0.045	+0.033	+0.015	+0.012	+0.021
$\log \rho_c/\bar{\rho}$ .....	+2.86	+3.628	+3.960	+4.541	+5.861	+6.244	+5.770

a Roman numeral. The few particular jump lines whose upper end-points do not fall on a numerical solution for the intermediate zone were obtained by interpolation between the available numerical solutions. Altogether, seven particular models were thus derived for the first series and eight for the second series, all of which are shown in Figure 1.

After the models had been completed in terms of the  $U$ - $V$  plane, the remaining non-dimensional characteristics were obtained in the following sequence. With the help of the values of  $U_{2e}$  and  $V_{2e}$ , graphic interpolation between the tabulated envelope solutions gave directly  $C$ ,  $t_2$ ,  $p_2$ ,  $q_2$ , and  $x_2$ . Next the ratio  $t_2/t_1$  was read from the intermediate-zone solution, since for this zone the starting point  $(U_1, V_1)$  and the end-point  $(U_{2i}, V_{2i})$  had already been determined. This ratio, together with the previously found value of  $t_2$ , gave the value of  $t_1$ . The values of  $p_1$ ,  $q_1$ , and  $x_1$  were then determined from equations (8) with the help of the known quantities  $U_1$ ,  $V_1$ ,  $n_1$ , and  $t_1$ . Finally,  $t_c$  and  $p_c$  were computed with the help of the first two equations (9) by applying these equations to the inner inter-

face (subscript 1); here the values for  $t_1$  and  $p_1$  previously found were used, together with the value for  $\theta_1$  read from the tabulated solution for the convective core in accordance with the  $\xi_1$  value characteristic of the particular model.

All these nondimensional quantities are listed in Table 1 for the first series of models and in Table 2 for the second series.

## IV. PHYSICAL CHARACTERISTICS OF MODELS

Five of the physical characteristics of interest are completely determined by the model as derived in the previous section and do not depend on any specific properties

TABLE 2  
MATHEMATICAL CHARACTERISTICS OF SECOND-MODEL SERIES

	I	II	III	IV	V	VI	VII	VIII
$\xi_1$ .....	+1.1400	+1.1250	+1.1213	+1.1204	+1.12012	+ 1.120097	+ 1.120093	+ 1.120092
$U_1$ .....	+2.618	+2.628	+2.631	+2.631	+2.631	+ 2.631	+ 2.631	+ 2.631
$V_1$ .....	+1.112	+1.082	+1.075	+1.073	+1.072	+ 1.072	+ 1.072	+ 1.072
$U_{2e}$ .....	+0.718	+0.582	+0.441	+0.324	+0.190	+ 0.127	+ 0.110	+ 0.099
$V_{2e}$ .....	+1.417	+1.774	+2.181	+2.560	+3.140	+ 3.541	+ 3.690	+ 3.809
$(n+1)_{2e}$ .....	+3.283	+3.567	+3.803	+3.962	+4.115	+ 4.173	+ 4.187	+ 4.195
$\log C$ .....	-5.388	-5.140	-4.793	-4.427	-3.723	- 3.000	- 2.4	- 1.5
$\log t_2$ .....	+0.152	+0.248	+0.390	+0.578	+1.080	+ 1.80	+ 2.4	+ 2.8
$\log p_2$ .....	+2.649	+2.980	+3.455	+4.107	+5.934	+ 8.66	+10.9	+12.3
$\log q_2$ .....	-0.866	-0.738	-0.617	-0.530	-0.422	- 0.36	- 0.3	- 0.2
$\log x_2$ .....	-1.169	-1.235	-1.346	-1.516	-1.999	- 2.70	- 3.3	- 3.5
$\log t_2/t_1$ .....	-0.182	-0.245	-0.320	-0.395	-0.515	- 0.60	- 0.6	- 0.6
$\log t_1$ .....	+0.334	+0.493	+0.710	+0.973	+1.595	+ 2.40	+ 3.0	+ 3.4
$\log p_1$ .....	+3.144	+3.706	+4.477	+5.435	+7.764	+10.86	+13.3	+14.5
$\log q_1$ .....	-1.422	-1.402	-1.358	-1.311	-1.233	- 1.17	- 1.1	- 1.0
$\log x_1$ .....	-1.404	-1.531	-1.701	-1.917	-2.460	- 3.20	- 3.8	- 4.0
$\log t_c$ .....	+0.429	+0.586	+0.802	+1.065	+1.687	+ 2.49	+ 3.1	+ 3.5
$\log p_c$ .....	+3.382	+3.938	+4.707	+5.665	+7.994	+11.09	+13.5	+14.7
$q_1 = M_1/M$ ...	+0.038	+0.040	+0.044	+0.049	+0.058	+ 0.068	+ 0.08	+ 0.11
$q_2 = M_2/M$ ...	+0.136	+0.183	+0.242	+0.295	+0.378	+ 0.44	+ 0.5	+ 0.7
$x_1 = r_1/R$ .....	+0.039	+0.029	+0.020	+0.012	+0.0035	+ 0.0006	+ 0.0002	+ 0.0001
$x_2 = r_2/R$ .....	+0.068	+0.058	+0.045	+0.030	+0.010	+ 0.002	+ 0.0005	+ 0.0003
$\log \rho_c/\bar{\rho}$ .....	+2.874	+3.273	+3.826	+4.521	+6.228	+ 8.52	+10.3	+11.1

of individual stars. These quantities are listed at the bottom of Tables 1 and 2; they are the fraction of the total mass contained in the convective core,  $q_1$ ; the fraction of the total mass contained in the hydrogen-poor interior (convective core and intermediate zone),  $q_2$ ; the fraction of the radius occupied by the convective core,  $x_1$ ; the fraction of the radius occupied by the hydrogen-poor interior,  $x_2$ ; and the ratio of central to mean density,  $\rho_c/\bar{\rho}$ .

The fraction of the mass contained in the hydrogen-poor interior,  $q_2$ , is the essential physical parameter which varies from model to model in each series. Tables 1 and 2 show that the computed models cover a large range in  $q_2$ , each of the two series starting with a model containing less than 14 per cent of the mass in the interior and ending with a model containing over 70 per cent in the interior.

The values listed for  $x_2$  show that the hydrogen-poor interior, though containing in

many cases a large fraction of the mass, occupies at most a few per cent of the radius of the star. This indicates a high central concentration of these models, which is explicitly shown by the values for  $\log \rho_c/\bar{\rho}$  listed.

To derive further physical characteristics for the model stars here considered, it is necessary to apply the models described in the previous section to specific cases characterized by definite values for the mass, the composition, the central temperature, and the guillotine factor. Correspondingly, the subsequent computations are based on the following assumptions. The internal composition is arbitrarily taken to be  $X_i = 0.01$ ,  $Y_i = 0.97$ , and  $Z_i = 0.02$ , while the envelope composition is assumed to be  $X_e = 0.92$ ,  $Y_e = 0.06$ , and  $Z_e = 0.02$ . These compositions correspond to the numerical values of  $l_i$  and  $j_i$  used in the construction of the models. Further,  $(t/\bar{g})_0 = 2$  has been used for the guillotine factor law given by equation (2). Finally, the central temperature was assumed to be  $3 \times 10^7$  °K throughout. This last assumption is a substitute for an accurate evaluation of the central temperature needed by the carbon cycle to produce the required energy; such computations did not seem worth while at the present state of these models and the present uncertainty in the carbon-cycle cross-sections. Finally, regarding the assumed stellar masses, the first series of models was applied only to stars of two solar masses, while the second series was applied to stars of one, two, and four solar masses.

Under these assumptions the physical characteristics were computed in the following sequence.

To start with, the radius of a particular model star could be obtained from the second of equations (3) by applying this equation to the center of the star; the radius is the only unknown quantity in this equation, since  $T_c$ ,  $\mu_e$ , and  $M$  are given by the above assumptions, whereas  $t_c$  can be taken from Table 1 or Table 2 for any specific model. Similarly, the luminosity could be found from equation (7). With  $R$  and  $L$  known, the effective temperature,  $T_e$ , could be obtained from its usual definition. Finally, the temperatures at the two interfaces and the densities at the center and at the two interfaces could be computed directly from the first two of equations (3)—together with the equation of state—since the nondimensional values  $p$  and  $t$  corresponding to these particular locations are listed in Tables 1 and 2.

The physical characteristics enumerated above are given in Tables 3 and 4 for models of the first and second series, respectively.

#### V. CHECKS ON ASSUMPTIONS

After the physical properties of the model stars were derived, it was possible to check some of the assumptions on which the computations had been based. These checks were performed on a typical case represented by model V of the first series as applied to a star of two solar masses. For this case temperatures and densities were computed for a number of points throughout the star; these are given in Table 5.

The first check concerns equation (2), the law assumed for the guillotine factor. From Morse's table of the guillotine factor for Russell mixture,<sup>7</sup> the guillotine factor was obtained for the temperatures and densities in question and is listed in the fifth column of Table 5. These values for the guillotine factor are also shown as a function of the density by the solid line in Figure 2. The dashed lines in the same figure represent the guillotine factor, as assumed for the models according to equation (2). The figure shows that in the envelope the assumed law is quite representative. In the interior, however, the assumption used for the models of the first series gives appreciably too low a guillotine factor, while the assumption for the second series is apparently much more representative. For future computations a still further increase in the guillotine factor for the interior seems to be indicated by Figure 2—not so much in the slope ( $\alpha$ ) as in the constant factor  $(t/\bar{g})_0$ .

<sup>7</sup> P. M. Morse, *Ap. J.*, **92**, 27, 1940.

TABLE 3  
PHYSICAL CHARACTERISTICS OF FIRST-MODEL SERIES  
( $M/M_{\odot} = 2$ )

	I	II	III	IV	V	VI	VII
$R/R_{\odot}$ .....	+ 2.19	+ 4.32	+ 5.85	+ 9.82	+32.7	+49.0	+40.2
$\log L/L_{\odot}$ .....	+ 0.87	+ 1.20	+ 1.36	+ 1.60	+ 2.22	+ 2.58	+ 3.12
$\log T_e$ .....	+ 3.80	+ 3.74	+ 3.72	+ 3.66	+ 3.56	+ 3.55	+ 3.74
$T_1 \times 10^{-6}$ .....	+23.3	+23.6	+23.6	+23.6	+23.6	+23.6	+23.6
$T_2 \times 10^{-6}$ .....	+15.7	+12.1	+11.0	+ 9.5	+ 7.4	+ 6.7	+ 5.9
$\log \rho_c$ .....	+ 2.29	+ 2.17	+ 2.11	+ 2.02	+ 1.77	+ 1.62	+ 1.41
$\log \rho_1$ .....	+ 2.13	+ 2.02	+ 1.95	+ 1.86	+ 1.61	+ 1.47	+ 1.25
$\log \rho_{2i}$ .....	+ 1.84	+ 1.38	+ 1.19	+ 0.91	+ 0.32	+ 0.04	- 0.36
$\log \rho_{2e}$ .....	+ 1.44	+ 0.98	+ 0.79	+ 0.51	- 0.08	- 0.36	- 0.76

TABLE 4  
PHYSICAL CHARACTERISTICS OF SECOND-MODEL SERIES

	I	II	III	IV	V	VI	VII	VIII
$M/M_{\odot}=1.0$								
$R/R_{\odot}$ .....	+ 1.09	+ 1.57	+ 2.58	+ 4.72	+19.8	+126	+530	+1300
$\log L/L_{\odot}$ .....	- 0.646	- 0.477	- 0.238	- 0.003	+ 0.390	+ 0.711	+ 1.000	+ 1.71
$\log T_e$ .....	+ 3.580	+ 3.544	+ 3.495	+ 3.423	+ 3.210	+ 2.888	+ 2.646	+ 2.63
$T_1 \times 10^{-6}$ .....	+24.1	+24.2	+24.3	+24.3	+24.3	+24.4	+23	+24
$T_2 \times 10^{-6}$ .....	+15.8	+13.8	+11.6	+ 9.8	+ 7.4	+ 6.1	+ 5.7	+ 6.0
$\log \rho_c$ .....	+ 2.91	+ 2.84	+ 2.74	+ 2.65	+ 2.49	+ 2.37	+ 2.3	+ 1.9
$\log \rho_1$ .....	+ 2.77	+ 2.70	+ 2.60	+ 2.51	+ 2.35	+ 2.23	+ 2.2	+ 1.8
$\log \rho_{2i}$ .....	+ 2.45	+ 2.22	+ 1.90	+ 1.58	+ 1.04	+ 0.63	+ 0.4	+ 0.2
$\log \rho_{2e}$ .....	+ 2.05	+ 1.82	+ 1.50	+ 1.18	+ 0.64	+ 0.23	+ 0.0	- 0.2
$M/M_{\odot}=2$								
$R/R_{\odot}$ .....	+ 2.18	+ 3.13	+ 5.15	+ 9.44	+39.5	+250	+1100	+2600
$\log L/L_{\odot}$ .....	+ 0.859	+ 1.028	+ 1.268	+ 1.502	+ 1.895	+ 2.216	+ 2.501	+ 3.211
$\log T_e$ .....	+ 3.806	+ 3.770	+ 3.721	+ 3.648	+ 3.436	+ 3.114	+ 2.872	+ 2.858
$T_1 \times 10^{-6}$ .....	+24.1	+24.2	+24.3	+24.3	+24.3	+24.4	+23	+24
$T_2 \times 10^{-6}$ .....	+15.8	+13.8	+11.6	+ 9.8	+ 7.4	+ 6.1	+ 5.7	+ 6.0
$\log \rho_c$ .....	+ 2.31	+ 2.24	+ 2.14	+ 2.05	+ 1.89	+ 1.77	+ 1.7	+ 1.3
$\log \rho_1$ .....	+ 2.16	+ 2.10	+ 2.00	+ 1.91	+ 1.75	+ 1.63	+ 1.6	+ 1.2
$\log \rho_{2i}$ .....	+ 1.85	+ 1.62	+ 1.30	+ 0.98	+ 0.43	+ 0.03	- 0.2	- 0.4
$\log \rho_{2e}$ .....	+ 1.45	+ 1.22	+ 0.90	+ 0.58	+ 0.03	- 0.37	- 0.6	- 0.8
$M/M_{\odot}=4$								
$R/R_{\odot}$ .....	+ 4.37	+ 6.27	+10.3	+18.9	+79.1	+500	+2100	+5100
$\log L/L_{\odot}$ .....	+ 2.364	+ 2.533	+ 2.773	+ 3.007	+ 3.400	+ 3.721	+ 4.010	+ 4.716
$\log T_e$ .....	+ 4.031	+ 3.996	+ 3.946	+ 3.875	+ 3.661	+ 3.340	+ 3.098	+ 3.084
$T_1 \times 10^{-6}$ .....	+24.1	+24.2	+24.3	+24.3	+24.3	+24.4	+23	+24
$T_2 \times 10^{-6}$ .....	+15.8	+13.8	+11.6	+ 9.8	+ 7.4	+ 6.1	+ 5.7	+ 6.0
$\log \rho_c$ .....	+ 1.70	+ 1.63	+ 1.54	+ 1.44	+ 1.29	+ 1.17	+ 1.1	+ 0.7
$\log \rho_1$ .....	+ 1.56	+ 1.49	+ 1.40	+ 1.31	+ 1.15	+ 1.03	+ 1.0	+ 0.6
$\log \rho_{2i}$ .....	+ 1.25	+ 1.01	+ 0.70	+ 0.37	- 0.17	- 0.57	- 0.8	- 1.0
$\log \rho_{2e}$ .....	+ 0.85	+ 0.61	+ 0.30	- 0.03	- 0.57	- 0.97	- 1.2	- 1.4

The second check refers to the neglect of electron scattering. The sixth column in Table 5 gives the ratio of the absorption coefficient here used, according to equations (1) and (2), to the absorption coefficient arising from electron scattering. The values given are computed for the same typical case used in the first check. The tabulation shows that—except in the convective core, where the absorption coefficient has no effect on the conditions—electron scattering provides less absorption than photoionization. However, electron scattering is not much less important than photoionization, at least in the inner portions of the star. Nevertheless, for the typical case represented by Table 5, the error

TABLE 5  
GUILLOTINE FACTOR, ELECTRON SCATTERING, AND RADIATION  
PRESSURE IN TYPICAL MODEL STAR

$r/R$	$M_r/M$	$\log T$	$\log \rho$	$\log (l/\bar{g})$	$\kappa/\kappa_e$	$P_g/P_r$
0.0 . . . . .	+0.00	+7.477	+1.77	+1.07	+0.8	+ 54
$x_1=0.005$ . . . . .	+0.08	+7.372	+1.61	+0.90	+1.3	+ 78
$x_{2i}=0.015$ . . . . .	+0.49	+6.867	+0.32	+0.47	+3.8	+130
$x_{2e}=0.015$ . . . . .	+0.49	+6.867	-0.08	+0.40	+1.5	+130
0.1 . . . . .	+0.78	+6.16	-2.26	+0.24	+3.0	+110
0.2 . . . . .	+0.91	+5.83	-3.28	.....	+4.1	+100
0.3 . . . . .	+0.96	+5.60	-4.00	.....	+5.0	+ 98
0.4 . . . . .	+0.98	+5.42	-4.62	.....	+5.1	+ 81
0.5 . . . . .	+0.99	+5.24	-5.18	.....	+6.0	+ 78
0.6 . . . . .	+1.00	+5.07	-5.75	.....	+6.4	+ 68
0.7 . . . . .	+1.00	+4.88	-6.38	.....	+6.9	+ 59

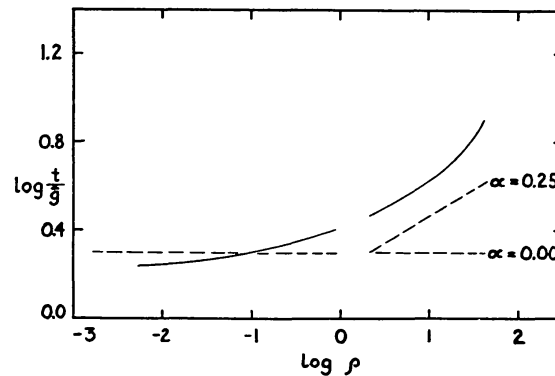


FIG. 2.—The guillotine factor through the star as a function of density. The solid line is the value as determined for the typical case of model *V* of the first series for a star of 2 solar masses. The dashed lines are the assumed representations for the models. In the interior, the dashed line marked “ $\alpha = 0$ ” represents the first-model series, while the line “ $\alpha = 0.25$ ” denotes the second-model series.

produced by neglecting electron scattering does not appear serious and is partially compensated for by the use of too small a guillotine factor, as discussed above. For heavier giants, however, the relative importance of electron scattering increases (proportional to  $M^2$ ), and an appropriate combination of photoionization and electron scattering will eventually have to be taken into account.

The third check refers to the neglect of radiation pressure. The last column of Table 5 gives the ratio of gas pressure to radiation pressure for the typical case used above. The tabulation shows that radiation pressure plays virtually no role throughout the body of the star considered. Since the relative importance of radiation pressure varies with  $M^2$ ,

a red giant has to have a mass of 10 solar masses or more if radiation pressure is to become really important.

The fourth check refers to the neglect of degeneracy. If in a diagram<sup>8</sup> showing the  $\log T - \log \rho$  plane, the demarcation line between degeneracy and nondegeneracy is drawn and if, in the same diagram, the data of the third and fourth columns of Table 5 are plotted, it is found that the entire typical model star represented by Table 5, including its center, falls in the nondegenerate region. The same is found to be essentially true for all the other model stars here considered, as can be seen from the  $\rho_c$  values of Tables 3 and 4.

The final check concerns the assumed central temperature of  $3 \times 10^7$ ° K. Again choosing the same typical model, an integration of the energy generation law for the carbon cycle shows that the assumed temperature cannot be much in error if the recent estimates<sup>9</sup> of the rate of the carbon cycle are essentially correct.

In summarizing these checks, it appears that the actual physical conditions in stars possessing the assumed composition discontinuity are satisfactorily represented by the second series of models as long as these models are not applied to too heavy giants. The first series of models appears to underestimate the guillotine factor in the deep interior; however, the comparison of this first series with the second series is useful in showing which of the results depend sensitively on the detailed behavior of the absorption coefficient in the deep interior.

#### VI. HERTZSPRUNG-RUSSELL DIAGRAM

To facilitate the comparison between the present model stars and observations, the model stars described above are presented in Figure 3 in terms of the Hertzsprung-Russell diagram.

Each case of Tables 3 and 4 is plotted in Figure 3 according to its values for the luminosity and the effective temperature. Each of the three heavy lines in the center and right-hand portions of the diagram represents all the models of the second series as applied to a definite stellar mass; the bottom line corresponds to 1 solar mass, the middle line to 2 solar masses, and the top line to 4 solar masses. Each of the dashed lines crossing the solid lines corresponds to a particular model of the second series as applied to various stellar masses. Since each model has a definite fraction of the total mass in the hydrogen-poor interior, the dashed lines indicate the progression of hydrogen exhaustion; at the lower left the mass fraction in the hydrogen-poor interior is small, whereas in the upper right portion it is large.

For comparison the locations of actually observed giants, subgiants, and main-sequence stars are very approximately indicated by the shaded areas.

Figure 3 shows that the models here considered amply cover the territory in the Hertzsprung-Russell diagram occupied by the red giants. Indeed, the most extreme models of the second series give effective temperatures probably lower than that of any observed star.

How sensitively the effective temperature of a star, i.e., its radius, depends on the exact run of the absorption coefficient in the deep interior is shown by the thin solid line which represents the first series of models as applied to stars of 2 solar masses. According to this series, a star of 2 solar masses reaches its lowest effective temperature at about 3500° K, while the same star, according to the second series, can reach an effective temperature below 1000° K. Therefore, to predict accurately the position in the Hertzsprung-Russell diagram of an inhomogeneous star, it will be necessary not only to specify in detail the character of the chemical inhomogeneity but also to represent the absorption coefficient in the interior with appreciable accuracy.

<sup>8</sup> G. W. Wares, *Ap. J.*, **100**, 158, 1944.

<sup>9</sup> I. Epstein, *Ap. J.*, **112**, 207, 1950.

To indicate the great difference in location in the Hertzsprung-Russell diagram between chemically homogeneous and inhomogeneous stars, the position of homogeneous stars with central temperatures of  $3 \times 10^7$ ° K is indicated by a set of lines in the left-hand part of Figure 3. Here again each solid line connects all points corresponding to a given stellar mass, while each dashed line corresponds to a given degree of hydrogen exhaustion. For the homogeneous models the degree of hydrogen exhaustion is given directly by the hydrogen abundance (assumed constant throughout the star) which decreases from 92 per cent near the middle of Figure 3 to 1 per cent near its left edge.

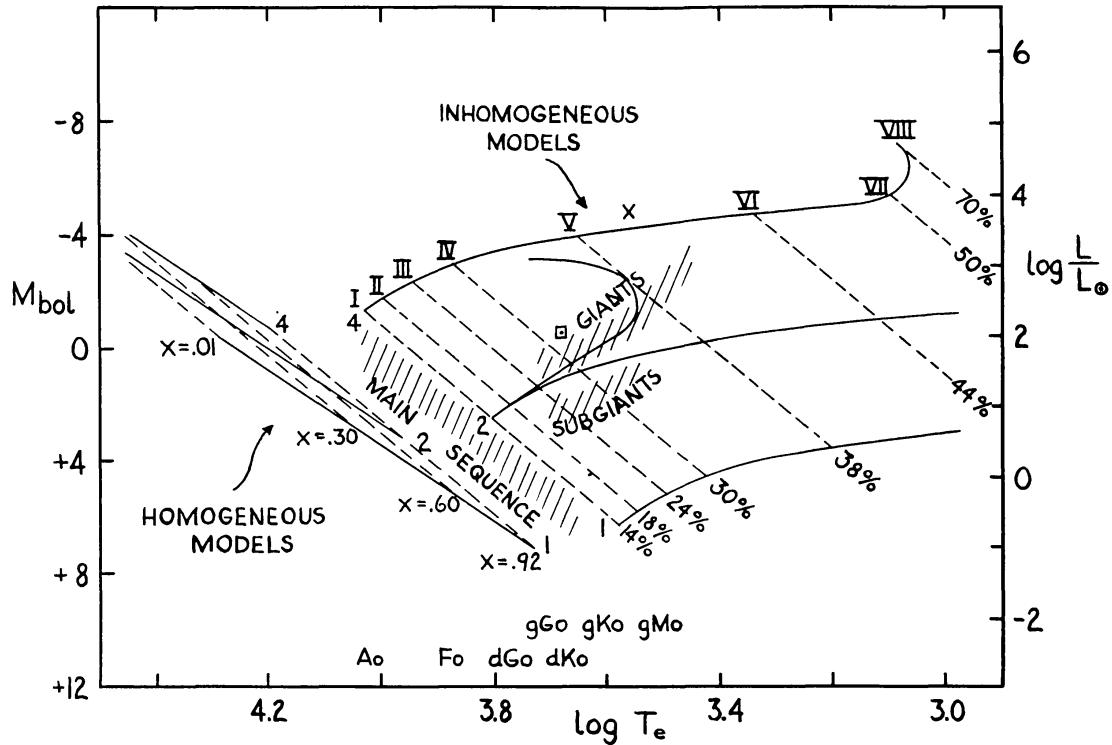


FIG. 3.—The Hertzsprung-Russell diagram for the models in terms of bolometric magnitude and effective temperature. The three heavy lines marked 1, 2, and 4 in the right part of the diagram represent the models of the second series applied to stars of 1, 2, and 4 solar masses. (The extra thin solid curve shows, for comparison, the line for 2 solar masses for the first-model series.) Each dashed line represents a specific model, which is marked by its Roman numeral and its percentage of the total mass in the hydrogen-poor interior. The solid and dashed lines to the left denote the corresponding homogeneous models. The hatched areas represent, approximately, the normal observed Hertzsprung-Russell diagram. The square and cross represent, respectively, the observed positions of Capella and  $\zeta$  Aurigae.

Figure 3 permits a rough estimate of the possible evolutionary track of a bright star through the upper portions of the Hertzsprung-Russell diagram. A star of, say, 2 solar masses will start approximately as an F0 star with a bolometric absolute magnitude of about +3. If this star contains strong mixing mechanisms and correspondingly remains chemically homogeneous throughout its life, it will evolve along the middle one of the solid lines in the left-hand part of Figure 3 and thus increase in both absolute magnitude and effective temperature. If, however, the same star contains only a limited mixing mechanism, which only successively reaches through larger and larger fractions of the stellar mass, then the star will evolve along the middle one of the solid lines in the right-hand portion of Figure 3. It will thus, while slowly increasing in luminosity and be-

coming redder and redder, reach a minimum in the effective temperature, after which it will increase its effective temperature again and, passing through the supergiant region, end as a bright-blue star—assuming that no new physical phenomena set in before the star has essentially exhausted all its hydrogen. The great difference in the evolutionary track through the Hertzsprung-Russell diagram for homogeneous and inhomogeneous stars shows that the strength and character of the internal mixing mechanisms play a decisive role in the apparent evolution of bright stars.

It is tempting to compare Figure 3 with the Hertzsprung-Russell diagram for a globular cluster under the assumption that the cluster stars are built according to the inhomogeneous models here considered. To derive for each star its present position along its evolutionary track, one has to take account of the difference in speed of evolution for stars of different luminosity or mass. Thus a star of 1 solar mass may still be essentially homogeneous; a star of 2 solar masses may already have developed the hydrogen-poor core containing, say, 15 per cent of the total stellar mass; and a star of 3 solar masses may already have extended its hydrogen-poor core to over 70 per cent of its total mass. If one draws a line through the three corresponding points in Figure 3, one obtains a curve which has some resemblance to the main branch of the Hertzsprung-Russell diagram of a globular cluster. It does, however, not seem warranted to follow this speculation at present into further detail, mainly because of the arbitrariness with which the character of the chemical inhomogeneity has been selected for the models here investigated.

#### VII. MASSES OF RED GIANTS

In the preceding section the present stellar models were compared with observations in terms of absolute magnitudes and effective temperatures. It remains to compare the theoretical models with observed stellar masses.

The direct observational data on masses of red giants appear to be still very restricted and uncertain. The best available data seem to be those for Capella and Zeta Aurigae. The red components of these two binaries are indicated in the Hertzsprung-Russell diagram of Figure 3 by a square and a cross, respectively. By interpolating in this diagram between the heavy lines which represent various stellar masses, one can read off mass values for the two stars. One thus obtains approximately 2.5 and 5 solar masses for the red components of Capella and Zeta Aurigae, respectively. These theoretical mass values, derived under the assumption that the present inhomogeneous models are applicable to the stars considered, are to be compared with the observational values.

For the red component of Capella the earlier observational value of 4 solar masses has recently been shown to be possibly too high. The new observations<sup>10</sup> give, with much uncertainty, a mass around 2.7 solar masses, which is in satisfactory agreement with the above theoretical value.

For the red component of Zeta Aurigae a mass of 15 solar masses or more has been derived from the observational data.<sup>11</sup> The discrepancy between this value and our theoretical value of 5 solar masses is very large indeed. The question arises whether the observational value could possibly be greatly in error. The observational mass is based on the determination of the mass function and the mass ratio. The mass function was derived from radial-velocity measurements of the K component, which has many sharp lines, on spectrograms which covered the entire orbit; accordingly, the mass function seems fairly secure. On the other hand, the mass ratio is derived from radial-velocity measurements of the B component, which has few and broad lines, on a small number of spectrograms, which in each of the three investigations in question covers only one

<sup>10</sup> Struve, *loc. cit.*

<sup>11</sup> W. Christie and O. Wilson, *Ap. J.*, **81**, 426, 1935.

particular phase of the orbital cycle. Accordingly, the mass ratio for Zeta Aurigae appears to be extremely uncertain. Instead of using the uncertain mass ratio, one might use the assumption that the B component of Zeta Aurigae falls on the mass-luminosity relation applicable for main-sequence stars. Thus one would get, for a bolometric magnitude of  $-1.4$ ,<sup>12</sup> a mass of 5 solar masses for the B component. The latter value, together with the observed mass function, would give 6 solar masses for the mass of the K component. This empirical value would be in excellent agreement with the theoretical value derived above. Whether, however, this interpretation of the observational data on Zeta Aurigae is correct can be decided only after a set of spectrograms covering the B component around an entire orbital cycle has been obtained.

In addition to the use of individual binaries with red-giant components, statistical data for whole groups of such binaries may be used to derive averaged masses of red giants.<sup>13</sup> Such averaged mass determinations for red giants appear, however, at present still very uncertain, as is indicated by the appreciable difference in the result, depending on whether trigonometric or spectroscopic parallaxes are used.

Besides the direct method of determining stellar masses from binaries, two indirect methods may be used for gaining information regarding the masses of red giants.

As a first method the period-density law for pulsating stars may be applied to cepheids. Since for cepheids the periods are very well known and the radii can be determined with fair accuracy from absolute magnitudes and effective temperatures, the theoretical period-density law can be used to determine the masses of cepheids. The resulting masses are, by a factor of approximately 3, smaller than those which are obtained if the mass-luminosity relation of main-sequence stars is applied to the cepheids.<sup>14</sup> This discrepancy has in the past been interpreted as indicating that the numerical coefficient in the theoretical period-density law must differ appreciably from the value thus far derived from pulsation theory. Now, however, it appears at least equally likely that one should interpret this discrepancy as indicating that the masses of cepheids are, in fact, appreciably smaller than had been inferred from the application of the mass-luminosity relation for main-sequence stars to cepheid variables.

As a second indirect method, one may derive the gravitational acceleration in the atmosphere of a star by a detailed analysis of the line strengths in its spectrum. When this method was first applied to giants and supergiants, values were found for the gravitational acceleration which were smaller by large factors than those derived from the mass-luminosity relation. This large discrepancy has since been greatly diminished, first, by introducing the  $H^-$  absorption, which increased the mean absorption coefficient, and, second, by introducing the turbulent velocities as deduced from line profiles, which increased the total kinetic temperature.<sup>15</sup> Nevertheless, the gravitational accelerations now derived are still smaller than those obtained from the mass-luminosity law of main-sequence stars by a factor of the order of 3. Perhaps this may be taken as further indication that the masses of the red giants are indeed somewhat smaller than those implied by the standard mass-luminosity relation.

In summarizing the observational data regarding the masses of red giants, one may conclude that the indirect evidence somewhat favors the relatively low masses required by the present inhomogeneous models and that the direct evidence does not necessarily contradict these low values.

<sup>12</sup> P. Wellmann, *A.N.*, **279**, 257, 1951.

<sup>13</sup> H. N. Russell and C. E. Moore, *The Masses of the Stars* (Chicago: University of Chicago Press, 1940).

<sup>14</sup> I. Epstein, *A.p. J.*, **112**, 6, 1950.

<sup>15</sup> O. C. Wilson, *A.p. J.*, **107**, 126, 1948; M. Schwarzschild, B. Schwarzschild, and W. S. Adams, *A.p. J.*, **108**, 207, 1948.

## VIII. SUMMARY

The inhomogeneous models described in detail in Sections III and IV and compared with observations in Sections VI and VII appear to cover well the observed ranges for red-giant stars, as far as luminosities and radii, i.e., position in the Hertzsprung-Russell diagram, are concerned.

The present models give masses for red giants which are smaller than those given by the mass-luminosity relation of main-sequence stars by factors of from 1.5 to about 3. The limited observational evidence on the masses of red giants, though in itself not suggesting a deviation from the regular mass-luminosity relation, still does not seem to be in direct discordance with these relatively low masses.

The two series of inhomogeneous models here described indicate that the evolutionary track of a bright star through the Hertzsprung-Russell diagram does depend sensitively both on the precise character of any chemical inhomogeneity and on the detailed run of the absorption coefficient in the deep interior. For stars with weak mixing mechanisms and an absorption law not too different from that of Kramers, the present models indicate an evolution which starts at the main sequence, passes through phases of increasing radius until a maximum size is reached, when the hydrogen-poor interior and the hydrogen-rich envelope are comparable in mass, and ends in a return toward the main sequence.

Stellar models like the present ones must still be considered as exploratory, owing to the arbitrariness with which the character of the chemical inhomogeneity is assumed. If, indeed, a chemical inhomogeneity is an essential feature in the internal structure of the red giants, as now appears likely, it will be possible to derive definite models for red giants only after the physical mechanisms which govern the degree and character of the internal mixing have been determined.